Spacecraft–Spacecraft Very Long Baseline Interferometry Part I: Error Modeling and Observable Accuracy

C. D. Edwards, Jr., and J. S. Border
Tracking Systems and Applications Section

In Part I of this two-part article, an error budget is presented for Earth-based delta differential one-way range (ΔDOR) measurements between two spacecraft. Such observations, made between a planetary orbiter (or lander) and another spacecraft approaching that planet, would provide a powerful target-relative angular tracking data type for approach navigation. Accuracies of better than 5 nrad should be possible for a pair of spacecraft with 8.4-GHz downlinks, incorporating 40-MHz DOR tone spacings, while accuracies approaching 1 nrad will be possible if the spacecraft incorporate 32-GHz downlinks with DOR tone spacings on the order of 250 MHz; these accuracies will be available for the last few weeks or months of planetary approach for typical Earth–Mars trajectories.

Operational advantages of this data type are discussed, and ground system requirements needed to enable spacecraft–spacecraft ΔDOR observations are outlined. This tracking technique could be demonstrated during the final approach phase of the Mars '94 mission, using Mars Observer as the in-orbit reference spacecraft, if the Russian spacecraft includes an 8.4-GHz downlink incorporating DOR tones. Part II of this article will present an analysis of predicted targeting accuracy for this scenario.

I. Introduction

Conventional differential very long baseline interferometry (ΔVLBI), as depicted in Fig. 1, provides angular tracking of an interplanetary spacecraft relative to one or more extragalactic radio sources (e.g., quasars). With respect to this quasar reference frame, which defines an inertial navigation reference system, Galileo-era delta differential one-way range (ΔDOR) observations between a spacecraft and an angularly nearby quasar can provide roughly 30-nrad angular accuracy,[1] while enhancements in recorded and spanned bandwidths may enable nanoradian-level accuracy in the future [1]. However, to take full advantage of the high accuracy of ΔVLBI measurements

[1] J. Border, "Analysis of ΔDOR and ΔDOD Measurement Errors for Mars Observer Using the DSN Narrow Channel Bandwidth VLBI System," JPL Interoffice Memorandum 335.1-90-026 (internal document), Jet Propulsion Laboratory, Pasadena, California, May 15, 1990.

for planet-relative targeting, one must also have comparably accurate knowledge of the planetary ephemeris in the radio reference frame. This knowledge is currently limited to about 50 nrad for the inner planets, due mostly to uncertainty in the overall orientation of the planetary ephemerides in the radio frame, with larger ephemeris uncertainties for the outer planets. A number of techniques (observations of the millisecond pulsar PSR 1937+214, timing measurements of planetary occultations of quasars, Phobos and Magellan ΔVLBI, and intercomparison of VLBI and lunar laser ranging observations) promise to improve this knowledge to about the 25-nrad level in the next few years. Nevertheless, this still represents a large error for angular navigation, as compared with the precision of the ΔVLBI observable.

An alternative for planetary approach navigation, depicted in Fig. 2, is to use a radio signal from an orbiter or lander already at the target planet as a VLBI navigation reference beacon for the approaching spacecraft. The ΔDOR observations can then be made between the two spacecraft directly, effectively replacing the quasar with the reference spacecraft. The sequence of missions to Mars embodied in the framework of the Space Exploration Initiative (SEI) will enable such tracking opportunities, providing a number of advantages over conventional spacecraft–quasar ΔDOR. First, the frame-tie problem is eliminated: The differential measurement between the approach spacecraft and the reference spacecraft (planetary orbiter or lander) provides a direct target-relative measurement of the approach spacecraft's position. Of course, the frame-tie and ephemeris errors are replaced by any uncertainty in the reference spacecraft's position, but these errors should be much smaller than typical frame-tie or planetary ephemeris errors. For example, Doppler data typically provide subkilometer planet-relative positions for planetary orbiters, while position errors for fixed landers should be at or below about 10 meters using new differential tracking data types [2].

A second advantage of this technique is that as the approach spacecraft nears the target planet, the angular separation between the approach spacecraft and the reference spacecraft will continually decrease. This will reduce the size of a number of error sources, including platform errors (i.e., station location and Earth orientation) and propagation media effects. Thus, the highest quality data will be obtained just when it is most needed—immediately prior to orbit insertion.

Finally, because the spacecraft signals are deterministic, one-way spacecraft range observables can be generated locally at each station, without the need for the wideband data transfer and cross-correlation between stations that is required for generating a quasar group delay observable. Only simple carrier phase tracking of several sinusoidal tones from each spacecraft is required. This has several advantages in terms of efficiency and reliability, including real-time validation of successful signal reception and real-time generation of spacecraft phase and delay observables at each station, as well as near-real-time generation of station-differenced delays. Only a very small amount of data must be brought together to form the station-differenced observables (for example, the time-tagged spacecraft phases at a one-hertz rate) and so, in principle, the spacecraft–spacecraft ΔDOR observable could be available within minutes of the actual observation for input into a navigation filter.

A goal of this article is to examine the error budget for spacecraft-to-spacecraft ΔDOR. Each physical error source is examined and, to the extent possible, parameterized as a function of angular separation. The total angular tracking error as a function of spacecraft angular separation is then calculated for spacecraft with DOR tones at either X-band (8.4 GHz) or Ka-band (32 GHz.) Possible applications of this technique are discussed. In particular, an early opportunity to demonstrate spacecraft–spacecraft ΔDOR will present itself in September 1995, the tentative arrival date of the Russian Mars '94 mission at Mars, where the U.S. Mars Observer spacecraft will already have been in orbit for over two years. To evaluate the potential navigation improvement for this Mars '94 approach scenario, a covariance analysis is performed in Section II of this article, which is based on the spacecraft–spacecraft ΔDOR error budget.

II. Error Analysis

A. Observation Description

The nominal observation scenario considered here consists of three scans: a 60-sec observation of spacecraft A, then a 120-sec observation of spacecraft B, and finally another 60-sec observation of spacecraft A, with slew times of 60 sec allowed between scans. For each observation, two stations spanning an intercontinental baseline simultaneously observe a number of sinusoidal tones (referred to as DOR tones) from one of the spacecraft, which provides a group delay measurement of the difference in arrival times of that spacecraft's signal at two tracking stations. A differential observable is then formed by interpolating the two observations of spacecraft A to the epoch of the observation of spacecraft B, thereby eliminating any errors that are linear in time, and then differencing the interpolated delay for spacecraft A from the observed delay

for spacecraft B. These observation times are long enough to provide sufficient signal-to-noise ratio (SNR) for typical DOR tone amplitudes, yet short enough to keep various stochastic errors small. Two spacecraft configurations will be considered: a pair of spacecraft with X-band DOR tones (with a spanned bandwidth of $\Delta\nu_{DOR} = 40$ MHz) or a pair of spacecraft with Ka-band DOR tones ($\Delta\nu_{DOR} = 250$ MHz). (Additional DOR tones with smaller spanned bandwidths could be added to the spacecraft downlink spectrum, as required, to enable reliable ambiguity resolution.)

The mean elevation of the two spacecraft at each station will be assumed to be 20 deg, and the angular separation between the two spacecraft will be assumed to be solely in the elevation direction, providing a worst-case estimate of propagation media errors. Table 1 summarizes the observation description. This article considers spacecraft–spacecraft angular separations ranging from 0–20 deg on the sky plane.

At each station, two (or more) DOR tones from each spacecraft must be tracked to form the spacecraft DOR group delay observables. A multichannel closed-loop digital tracking receiver will simultaneously phase track all the tones from both spacecraft. While this capability does not currently exist in NASA's operational Deep Space Network (DSN), a demonstration is underway to use modified Global Positioning System (GPS) digital tracking receivers to simultaneously track carrier tones from Pioneer Venus Orbiter and Magellan at two stations [2]. Planned upgrades of the operational VLBI system will incorporate this capability. The closed-loop tracking provides a much lower data rate relative to current open-loop recording, and the multichannel capability provides higher SNR by eliminating time-multiplexing among DOR channels.

The actual spacecraft–spacecraft ΔDOR observable is obtained by combining the measured phases as follows: Let ν_{ij} represent the frequency of the ith DOR tone for spacecraft j, and let ϕ_{ijk} be the measured phase for that DOR tone at station k. The single-station one-way delay for spacecraft j at station k can then be obtained from a pair of DOR tones

$$\tau_{jk} = \frac{\phi_{2jk} - \phi_{1jk}}{\nu_{2j} - \nu_{1j}}$$

This one-way delay contains a bias due to uncertainty in the time of transmission of the signal from the spacecraft. By differencing this one-way observable between two ground stations, this bias is eliminated. The unbiased, station-differenced delay observable for spacecraft j is then

$$\tau_j = \tau_{j2} - \tau_{j1}$$

Interpolating the two observations of spacecraft A (at $t = -T$ and $t = +T$, respectively) to the epoch of the observation of spacecraft B (at $t = 0$), and then differencing between spacecraft, yields the final spacecraft–spacecraft ΔDOR observable

$$\tau = \frac{1}{2}(\tau_A(-T) + \tau_A(T)) - \tau_B(0)$$

(The simple arithmetic mean of the two observations of spacecraft A is appropriate in the absence of significant angular accelerations for spacecraft A. A more general interpolation scheme could be used to account for any large accelerations.)

This observable represents a measure of the geometric delay τ_g, which is a function of the relative angular position of the two spacecraft

$$\tau_g = \frac{1}{c}\vec{B} \cdot (\hat{s}_A - \hat{s}_B)$$

where $\hat{s}_A$ and $\hat{s}_B$ are the unit vectors in the directions of the two spacecraft, $\vec{B}$ is the baseline vector between ground antennas, and c is the speed of light.

In the next section, various error sources which corrupt this spacecraft–spacecraft ΔDOR observable will be examined. Each error source will be characterized in units that are most natural for the physical source of error, but ultimately one is interested in the angular error incurred on DSN intercontinental baselines. The following conversion factors will be used to relate various physical errors to an angular error on the sky plane:

1-cm path delay error = 33-psec delay error
= 1.67-nrad angular error

(This assumes a 6000-km projected length of the DSN intercontinental baseline on the sky plane.)

B. Error Components

1. Spacecraft Signal-to-Noise Ratio. The phase error σ_ϕ in the determination of the spacecraft tone phase is related to the SNR of the received DOR tone. The received DOR tone power can be expressed

$$P_{DOR} = P_{S/C}\ \zeta_{DOR}\ g_{S/C} \frac{\lambda^2}{(4\pi R)^2}\ g_{DSN}$$

where

$P_{S/C}$ = total transmitted spacecraft power

ζ_{DOR} = fraction of spacecraft power in the DOR tone (depends on modulation index and telemetry status)

$g_{S/C}$ = spacecraft antenna gain

λ = RF wavelength

R = Earth–spacecraft range

g_{DSN} = DSN ground antenna gain

In considering DOR tone SNR, the Mars Observer spacecraft will be used as a strawman configuration.[2] At maximum Earth–Mars range, with telemetry on (with an 80-deg modulation index), a 34-m high-efficiency DSN antenna provides a received DOR tone power of $P_{DOR} = -159.0$ dBm. The noise power per unit bandwidth is given by kT_{sys}, where k is Boltzmann's constant and T_{sys} is the system temperature of the receiving system, which represents the sum of the noise temperature of the first-stage amplifier, the brightness temperature of the atmosphere in the direction of the spacecraft, the 2.7-K cosmic background radiation, and any ground pickup from antenna spillover. Assuming a total noise system temperature of 25 K at X-band yields an X-band noise power per unit bandwidth of −184.6 dBm/Hz. The ratio of P_{DOR} to kT_{sys}, which describes the achievable link SNR in a one-second integration, is thus 25.6 dB-Hz.

The thermal phase error on the measured DOR tone phase is then given roughly by

$$\sigma_\phi = \sqrt{\frac{kT_{sys}}{P_{DOR} 2\tau_{int}}}\ \text{rad}$$

where τ_{int} is the integration time of the observation. For the 120-sec integrations for each spacecraft assumed here, one arrives at a phase error of 5.4×10^{-4} cycles at X-band. (For the purposes of treating the statistical error due to SNR, one can treat the two 60-sec observations of spacecraft A as a single 120-sec scan at the same epoch as the observation of spacecraft B.) The final thermal delay error is thus given by

$$\sigma_\tau = \sqrt{2 \times 2 \times 2}\ \frac{\sigma_\phi}{\Delta\nu_{DOR}}$$

where the three factors of $\sqrt{2}$ reflect the pairwise differencing between DOR tones, stations, and spacecraft, resulting in an X-band delay error of 38.3 psec.

If one assumes a similar ratio of P_{DOR} to T_{sys} at Ka-band (which provides a reasonable figure of merit in designing the Ka-band DOR transponder), then one obtains an equivalent phase error for Ka-band VLBI. The resulting delay error would then be 6.1 psec due to the larger Ka-band spanned bandwidth.

2. Ground System Instrumental Dispersion. Uncalibrated phase dispersion in the ground receiving instrumentation induces errors in the measured tone phases that will corrupt the final spacecraft–spacecraft ΔDOR observable. As other error sources are reduced due to high SNR and common-mode cancellation of media effects, these dispersive errors may well represent a limiting error source for spacecraft–spacecraft ΔDOR. With current VLBI instrumentation, preliminary studies indicate that dispersive errors are at the 1- to 2-deg level,[3] although more data on this error source are sorely needed. Achieving this level of phase error requires the use of phase calibration tones and/or the careful selection of a baseband frequency configuration to cancel instrumental errors between DOR tone channels.

A next-generation VLBI system employing broadband digitization of the entire intermediate frequency bandwidth and digital baseband filtering could significantly reduce instrumental errors by eliminating the analog baseband components that currently generate much of the dispersive phase effects. Design goals for this system provide for a one-millicycle dispersive phase error. The authors take this as the assumed instrumental dispersive phase error for each tone phase measurement. The resulting error in the spacecraft–spacecraft ΔDOR delay observable is

[2] Ibid.

[3] C. D. Edwards and K. Zukor, "Video Converter Local Oscillator Stability for Block I and Block II VLBI," JPL Interoffice Memorandum 335.1-90-055 (internal document), Jet Propulsion Laboratory, Pasadena, California, October 30, 1990.

$$\sigma_\tau = \sqrt{2 \times 2 \times 2}\ \frac{\sigma_\phi^{inst}}{\Delta\nu_{DOR}}$$

where the three factors of $\sqrt{2}$ again account for the pairwise differencing between DOR tones, stations, and spacecraft. This points out an important advantage of the increased spanned bandwidth available at Ka-band: For a given level of phase dispersion, delay errors are reduced proportional to the DOR tone spanned bandwidth. Assuming that $\sigma_\phi^{inst} = 1$ mcyc yields a σ_τ of 70.7 psec at X-band and 11.3 psec at Ka-band. At the smallest spacecraft angular separations, this error source will be one of the dominant contributors to the spacecraft–spacecraft ΔDOR error budget.

3. Station Clock Stability. Here the term "clock stability" represents both the stability of the station clock reference and the stability of the station frequency and timing distribution systems. The group delay error due to clock instability is on the order of

$$\Delta\tau = \sqrt{2} \times \sigma_y(\tau = 150 \text{ sec}) \times 150 \text{ sec}$$

where 150 sec is the time between central epochs of the scans for spacecraft A and B, and $\sigma_y(\tau = 150$ sec) is the Allan standard deviation, or fractional frequency stability, evaluated at this time separation. Assuming a station stability of $\sigma_y(\tau = 150 \text{ sec}) = 10^{-14}$, this yields a spacecraft–spacecraft ΔDOR delay error of 2.1 psec. For a flicker-frequency noise spectrum, this error will grow linearly with the temporal scan separation.

4. Troposphere. The troposphere error can be separated into a static component and a fluctuating component. The static component represents the error made in the context of a static, isotropic refractivity distribution characterized by a single zenith troposphere delay. The delay at an arbitrary elevation angle θ is related to this zenith value by a mapping function f_{map} that is approximated here as $1/\sin\theta$. At a single station, an error σ_τ^{zen} in the zenith troposphere will lead to a delay error when differencing between spacecraft

$$\sigma_\tau = \sigma_\tau^{zen} \left| \frac{1}{\sin\theta_A} - \frac{1}{\sin\theta_B} \right|$$

where θ_i is the elevation angle of spacecraft i. For the DSN stations, σ_τ^{zen} is currently about 4 cm, based on seasonal weather models and surface meteorology. Water vapor radiometers and/or global GPS tracking data should be able to provide reliable one-centimeter zenith troposphere estimates in the mid-1990s [3,4]; one centimeter will be used here as the representative zenith delay error. For two spacecraft with a mean elevation angle of 20 deg and angular separation $\Delta\theta$, assumed to be fully in the elevation direction, and accounting for uncorrelated one-centimeter zenith troposphere errors at each station, the resulting spacecraft–spacecraft ΔDOR delay error is

$$\sigma_\tau = \sqrt{2} \times 1 \text{ cm} \times \left| \frac{1}{\sin(20 \text{ deg} + \Delta\theta/2)} - \frac{1}{\sin(20 \text{ deg} - \Delta\theta/2)} \right|$$

In fact, the troposphere is neither static nor isotropic; spatial and temporal fluctuations, particularly in the distribution of atmospheric water vapor, lead to additional errors. Treuhaft and Lanyi [5] have developed a model of these fluctuations that is based on Kolmogorov turbulence. This model has been used to calculate the expected additional fluctuation error for the A-B-A scan sequence considered here, with the scans at a mean elevation of 20 deg and separated by 150 sec. The authors assume a tropospheric scale height of one kilometer, a wind speed of 8 m/sec, and a turbulence normalization constant of $2.4 \times 10^{-7} \text{m}^{-1/3}$ [5]. For a zero-degree angular separation, the effect of temporal fluctuations over the 150-sec scan separation times yields a fluctuation error of about 10 psec; as the angular separation is increased, the additional effect of spatial fluctuations becomes important, with the total fluctuation error reaching about 39 psec for a 20-deg angular separation.

While not assumed in this analysis, it should be mentioned that improved line-of-sight troposphere calibrations (using either improved WVRs or lidar calibration techniques) could ultimately reduce the total wet troposphere error to well below one centimeter, independent of angular separation.

5. Ionosphere. Dual-frequency downlinks on both spacecraft would enable charged particle–induced errors to be virtually eliminated from the spacecraft–spacecraft ΔDOR delay observable. For the analysis here, however, the authors assume only a single-band downlink and calculate the size of the charged particle error that is incurred. The total ionospheric delay along a given line of sight can be expressed

$$\tau_{[\text{psec}]}^{ion} = 1340 \times \frac{TEC_{[10^{16} \text{ el/m}^2]}}{\nu^2_{[\text{GHz}]}}$$

where TEC is the line-of-sight integrated total electron content, and all units are indicated [6]. As with the troposphere, one can also separate the ionospheric error into a "static" and a "fluctuating" component. The mapping function f_{map} used to express the elevation dependence of the static component differs slightly from the tropospheric mapping function, due to the height of the ionospheric shell above the Earth, and takes the form

$$f_{map} = 1/\sin\left(\cos^{-1}\left[\frac{\cos\theta}{1 + h/R}\right]\right)$$

where h is the height of the ionospheric shell above the Earth (~350 km) and R is the Earth's radius (~6371 km). The main impact is that the ionospheric mapping function increases more slowly at low elevations, saturating at a value of about 3.1 at the horizon. (This is a highly simplified picture of the ionosphere; in practice, the mapping function used is more complicated and accounts for the position of the Sun relative to the desired line of sight and the line of sight at which the ionospheric calibration was performed, in order to account for the diurnal variation in TEC. Nevertheless, the simple picture used here is adequate to estimate a typical error gradient on the sky due to ionospheric calibration error.) Using an analysis similar to that used for the troposphere shows that the static ionospheric error for the spacecraft–spacecraft ΔDOR delay observable is

$$\sigma_{\tau[\text{psec}]} = \sqrt{2} \times 1340 \times \frac{5}{\nu^2_{[\text{GHz}]}} \times |f_{map}(20 \text{ deg} + \Delta\theta/2) - f_{map}(20 \text{ deg} - \Delta\theta/2)|$$

where the authors have assumed an uncertainty in the zenith TEC of $\sigma_{TEC} = 5 \times 10^{16}$ el/m^2, and where the authors again take the worst-case geometry for which the spacecraft angular separation is entirely in the elevation direction. This corresponds to a 10-percent calibration uncertainty for a typical daytime maximum of $TEC = 50 \times 10^{16}$ el/m^2, which is consistent with ionospheric calibration accuracies using Faraday rotation or GPS satellite data. For $\Delta\theta = 5$ deg, this represents a delay error of 36 psec at X-band, or 2 psec at Ka-band.

The fluctuating component for the ionosphere is expected to be important, due to the variety of phenomena driving the ionospheric charged particle distribution (e.g., the day–night asymmetry, traveling ionospheric disturbances, and latitude variations) and the resulting limited accuracy of the simple static ionosphere model. Theoretical understanding of the processes driving ionospheric fluctuations is much less developed than for tropospheric fluctuations; as a result, empirical data will be used to guide the quantitative estimate of this error source. Based on a recent study that derives temporal fluctuation statistics from dual-frequency GPS carrier phase data,[4] an additional error of 0.5 TEC units (1 TEC unit = 10^{16} el/m^2) is specified to account for temporal ionospheric fluctuations at each site on the time scale of the differential observations. This level of fluctuation corresponds to a delay error of 13 psec at X-band and 0.9 psec at Ka-band.

6. Solar Plasma. Charged particles in the solar plasma also induce a delay error for spacecraft–spacecraft ΔDOR. The solar plasma delay error is proportional to the double-differenced line-of-sight integrated total electron content in the solar wind along the four relevant spacecraft–spacecraft ΔDOR lines of sight. The statistical model of Kahn and Border [7], based on solar plasma electron density spectra compiled by Woo and Armstrong [8], derives a spatial structure function for solar plasma-induced phase fluctuations, which can be used to calculate the error in the station-differenced delay to a single spacecraft

$$\sigma_\tau = \frac{134 \text{ psec}}{\nu^2_{[\text{GHz}]}[\sin SEP]^{1.225}}$$

where SEP is the Sun–Earth–probe angle. For spacecraft–spacecraft angular separations greater than about one degree, the solar plasma error for a second spacecraft will be essentially uncorrelated. Assuming a projected DSN baseline of 6000 km then yields a total spacecraft–spacecraft ΔDOR error of

$$\sigma_\theta = \frac{9.50 \text{ nrad}}{\nu^2_{[\text{GHz}]}[\sin SEP]^{1.225}}$$

A SEP angle of 20 deg for both spacecraft is assumed, which yields a total angular error of $\sigma_\theta = 0.50$ nrad at X-band and 0.03 nrad at Ka-band. Below a one-degree angular separation, the solar plasma error will be further reduced due to additional cancellation between raypaths for the two spacecraft.

7. Baseline Errors. Uncertainty in the baseline vector is due to a combination of a priori station location errors and errors in the knowledge of Earth orientation

[4] A. J. Mannucci, "Temporal Statistics of the Ionosphere," JPL Interoffice Memorandum 335.1-90-056 (internal document), Jet Propulsion Laboratory, Pasadena, California, October 25, 1990.

(UT1–UTC and polar motion). Any uncertainty $\delta\vec{B}$ in the baseline vector leads to a delay error

$$\delta\tau = \frac{1}{c}\delta\vec{B}\cdot(\hat{s}_1 - \hat{s}_2)$$

where $\hat{s}_1$ and $\hat{s}_2$ are the source directions to the two spacecraft. (In other words, the baseline path delay error is attenuated by the angular spacecraft separation, in radians, projected along the baseline direction.) It is assumed here that station coordinates in the terrestrial frame are known to 3 cm per component [9]. In addition, weekly VLBI observations combined with daily GPS observations have been shown to be able to deliver real-time Earth orientation estimates with 10-nrad accuracy [10]. Based on these two error components, a delay error of $\sigma_\tau = 4.3$ psec $\times\Delta\theta_{[\mathrm{deg}]}$ due to baseline uncertainty is specified.

8. Frame Tie. One final error contribution is related to the offset in the planetary and radio reference frames, and is referred to as the frame-tie uncertainty. In conventional spacecraft–quasar ΔVLBI, the spacecraft position is measured in the radio frame relative to a nearby quasar; the frame-tie offset contributes directly as an angular bias for determining the spacecraft position relative to a planetary target. The spacecraft–spacecraft ΔVLBI technique described in this article reduces the effect of the frame-tie error by directly measuring the approach spacecraft relative to a spacecraft at the target planet. Nonetheless, the frame tie does induce a small residual error in converting the measured ΔVLBI delay into an angular separation. The error is due to the fact that the baseline orientation is modeled in the radio reference frame, based on periodic VLBI and GPS measurements of Earth orientation, while the reference spacecraft's position is tied to the planetary ephemeris. The resulting angular error in the approach spacecraft's angular position relative to the target planet is proportional to the product of the frame-tie uncertainty and the angular separation between spacecraft, expressed in radians. The frame-tie uncertainty is currently about 50 nrad for the inner planets, but that value should be reduced to about 25 nrad based on several ongoing observational programs, including millisecond pulsar timing and VLBI observations [11], observations of planetary occultations of quasars [12], and joint solutions of VLBI and lunar laser ranging data sets [13]. Thus, the authors include an error in the determination of the approach spacecraft's target-relative position in terms of the spacecraft–spacecraft angular separation $\delta\theta$

$$\sigma_\theta = 25\ \mathrm{nrad} \times \frac{\pi}{180} \times \delta\theta_{[\mathrm{deg}]} = 0.44\ \mathrm{nrad} \times \delta\theta_{[\mathrm{deg}]}$$

C. The Total Spacecraft–Spacecraft ΔDOR Error Budget

Table 2 summarizes the error-modeling assumptions made in this analysis, while Tables 3 and 4 present the error budget for the X-band and Ka-band spacecraft–spacecraft ΔDOR cases considered here. Figure 3 summarizes the angular error for each case as a function of the angular separation between spacecraft. For the X-band case, the dominant errors for large angular separations (>10 deg) are the propagation media errors, due to uncertainties in the zenith troposphere and ionosphere delays. The angular error grows roughly by 0.7 nrad per degree of angular separation in this range. For smaller angular separations, the dominant errors are the small-scale fluctuations in the ionosphere and the instrumental phase dispersion, followed by troposphere fluctuations and the statistical measurement error due to the received spacecraft SNR. As the angular separation approaches zero, the accuracy levels out at just over 4 nrad.

The Ka-band error budget shows further accuracy improvement due to two factors. First, the much larger spanned bandwidth reduces the statistical measurement error as well as the phase dispersion error by a factor of 250/40 relative to the X-band case. Second, the higher Ka-band frequency reduces the effects of the ionosphere and the solar plasma by a factor of $(32/8.4)^2$, or about 14.5. For Ka-band, the dominant errors are troposphere and platform errors at large angular separations, and instrumentation and troposphere fluctuations at small angular separations.

III. Discussion

The error budget presented in the last section was parameterized as a function of the angular separation of the approach and in-orbit spacecraft. How does this angular separation evolve during the final weeks of planetary approach? As a representative example, consider the spacecraft–spacecraft angular separation for a Hohmann (minimum-energy) Earth–Mars transfer orbit. For this orbit, the Mars–Earth–probe (MEP) angle is less than 27 deg for essentially the entire trajectory, less than 10 deg for the last four months of the trajectory, and, in fact, less than 2 deg for the last 100 days. At encounter, the rate of change of the MEP angle is only 0.044 deg/day.

Higher energy transfer orbits, for which aerocapture insertions might be a key component, and therefore which may require highest accuracy approach navigation, will typically have larger approach velocities, but should still

have a spacecraft–planet angular separation of less than 5 deg for at least the last few weeks of planetary approach. Hence, the highest accuracy spacecraft–spacecraft ΔDOR observables will be available during the final critical targeting maneuvers in the last few weeks prior to encounter.

It should also be mentioned that during the final hours of planetary approach, the in-orbit and approach spacecraft will become sufficiently close on the sky plane that they may be observed simultaneously within a single Earth-based antenna beamwidth. This enables the use of the same-beamwidth interferometry (SBI) technique [2,14], in which the simultaneous observation of both spacecraft leads to further significant error reductions, with accuracies of 10–100 prad possible if the RF phase observable can be resolved. The X-band and Ka-band beamwidths of a 34-m antenna are 60 and 16 mdeg, respectively; thus, for the Hohmann trajectory described above, X-band SBI observations will be possible for over a day before encounter, and Ka-band for about 8 hours prior to encounter. Konopliv and Wood [15] have already shown how the SBI observable can provide accurate Mars approach navigation during the final hours of approach, helping to enable aerocapture. The key message of the results presented here, however, is that even before SBI observations are possible, nonsimultaneous spacecraft–spacecraft ΔDOR observations can provide significant improvements in target-relative approach navigation for weeks or even months before encounter.

One important error source that applies to spacecraft–spacecraft ΔDOR was not included in the error budget presented here: namely, the uncertainty in the planet-relative position of the in-orbit reference spacecraft. This error depends very much on the type of orbit the reference spacecraft is in, the amount and quality of tracking data collected for the in-orbit spacecraft, and assumptions about limiting errors, such as uncertainties in the planetary gravity field. Preliminary navigation analysis for the Mars Observer mission, for example, indicates that one-kilometer orbit errors are expected immediately after orbit insertion. However, after several weeks of intensive Doppler tracking, the resulting improvement in the Mars gravity field should allow a reduction of orbit errors to about 200 meters.[5] A 200-m spacecraft position error corresponds to an angular error of 0.5–2.5 nrad, depending on the Earth–Mars range. For X-band observations, this error will not be dominant, but it will be an important error source for the higher accuracy Ka-band observations. Of course, if the reference spacecraft is, in fact, a beacon on the planetary surface, its position will be known to a much higher accuracy: Conventional range and Doppler data should be able to provide Mars-centered beacon position determination with 10-m accuracy in the spin radius and 100-m accuracy along the spin axis. In addition, SBI between the surface beacon and an orbiter could provide few-meter Mars-relative beacon position accuracy in all three components [16].

Some error sources which are important for conventional quasar-relative ΔDOR are eliminated or greatly reduced in spacecraft-only observations. In the previous section the authors discussed how the frame-tie error is greatly reduced in the spacecraft–spacecraft technique, relative to spacecraft–quasar ΔVLBI. Other important error sources for quasar-relative ΔDOR include the statistical uncertainty in the measurement of the quasar delay, any a priori uncertainty in the quasar position, and the effect of source structure on the quasar position. Because of the limited 250-KHz recorded bandwidth of the NCB VLBI system, the quasar delay measurement error is one of the limiting error sources for conventional ΔDOR. An additional impact of the low NCB sensitivity is that only bright quasars can be reliably observed: A minimum correlated flux density of 0.4 Jy is typically required for reliable detection with a pair of DSN antennas, one 70-m and one 34-m. Due to the limited number of useful sources, it is often necessary to use a quasar more than 10 deg from the spacecraft, with the result that Earth orientation and propagation media errors are increased.

Finally, a priori source positions are uncertain at the level of about 5 nrad, based on the current DSN quasar data set. Source position accuracies may improve further, toward one-nanoradian accuracy with the increasing amount of Mark III observations in the source catalog data set. However, it is suspected that source structure can cause few-nanoradian errors in apparent source position, varying with time as the quasar jet structure evolves, and also changing with observation geometry as the fringe orientation changes and different source features are resolved; this error source may pose a difficult obstacle to achieving nanoradian-level quasar positions. Over short periods of weeks or months, during which source structure is expected to remain nearly constant, it is possible to eliminate the source structure error in a relative sense among a series of ΔDOR observations by always observing the same quasar(s) at exactly the same hour angle(s) [1]. However, this poses scheduling constraints and still does not eliminate any overall source position error common to all observations.

[5] P. Esposito, S. Demcak, D. Roth, G. Bollman, and A. Halsell, "Mars Observer Project Navigation Plan," JPL D-3820 (internal document), Jet Propulsion Laboratory, Pasadena, California, June 15, 1990.

IV. Opportunities to Demonstrate Spacecraft–Spacecraft ΔDOR

To validate the error budget presented here and gain experience in acquiring and processing this data type, it would be valuable to find opportunities to demonstrate the spacecraft–spacecraft ΔDOR observation technique. To demonstrate the technique, one requires two angularly close spacecraft, each with downlinks at the same frequency band, including VLBI DOR tones. Two noteworthy opportunities are mentioned here. First, in January of 1994, Venus and Mars pass near each other on the sky plane. At this time, Magellan will be in orbit about Venus, and Mars Observer will have recently arrived at Mars. Mars Observer has a 38.25-MHz DOR tone bandwidth, and Magellan has a 30.72-MHz bandwidth consisting of the ±16th harmonics of the 960-KHz telemetry subcarrier. The two spacecraft will pass within about 0.3 deg of each other, with closest approach occuring on January 6, 1994. By acquiring a series of spacecraft–spacecraft ΔDOR observations over a several-week period, it should be possible to verify the accuracy of the spacecraft–spacecraft ΔDOR data type as a function of spacecraft angular separation. In addition, a subkilometer determination of the sky-plane components of the offset between Venus and Mars at this epoch would result, providing a valuable constraint on the relative orientation of the orbit planes of these two planets.

The second, and potentially more interesting, opportunity involves using the Mars Observer spacecraft as a spacecraft–spacecraft ΔDOR reference for planetary approach of the Russian Mars '94 spacecraft. Mars '94 tentatively plans a September 1995 Mars orbit insertion; this is near the end of the prime mission of Mars Observer, which will have arrived at Mars in August of 1993. Mars Observer incorporates a 38.25-MHz X-band DOR tone bandwidth; if the Russians incorporate a similar capability on their spacecraft, it would be possible to collect spacecraft–spacecraft ΔDOR data during Mars '94 approach. In Part II of this article, a covariance analysis will be presented to examine the navigation benefits of such an observation program for the Russian spacecraft. And of course, after encounter, one would also be interested in collecting SBI data, which have already been shown to have significant navigational benefits to both missions [2,14]. This scenario provides a unique opportunity to demonstrate multiple spacecraft tracking at Mars, where future, more ambitious aerocapture missions encompassed within the SEI will benefit from new, high-accuracy tracking techniques.

V. Summary

Spacecraft–spacecraft ΔDOR observations between an in-orbit spacecraft and another spacecraft approaching that planet can provide target-relative angular navigation with accuracies of about 4 nrad during the last weeks of planetary approach for spacecraft equipped with X-band transponders incorporating roughly 40-MHz DOR tone spacings. Accuracies approaching one nanaradian can be obtained by going to Ka-band downlinks with DOR tone spacings of several hundred megahertz. These accuracies correspond to an observation duration of only 6 minutes.

The spacecraft–spacecraft ΔDOR observable has the advantage of tying the approach spacecraft directly to the planetary target. In addition, because only spacecraft signals are used, no wideband quasar recording is required. As a result, data transfer and data processing are simplified, which enables these observables to be available in near-real-time. To enable efficient data collection, a key part of the DSN's planned VLBI system upgrade should be the implementation of ground tracking receivers that can simultaneously track multiple tones from each spacecraft. Reducing instrumental phase dispersion errors to the millicycle level will be an important design goal for this new system and should be achievable by using digital data acquisition techniques. Other key improvements in ground capabilities assumed in this analysis are a 1-cm zenith troposphere calibration capability and a 3-cm station location knowledge. In the 1995 time frame, GPS and/or WVRs should be capable of providing troposphere calibrations at this level, while VLBI, GPS, and LLR data should be able to provide the required level of station location accuracy.

Opportunities to demonstrate the spacecraft–spacecraft ΔDOR technique will arise in the next several years, first with fortuitous sky-plane flybys of unrelated deep space missions, such as Magellan and Mars Observer, and then in 1995 by the possibility of using differential observations of Mars Observer and Mars '94 to improve the planetary approach targeting for the Mars '94 mission.

Acknowledgments

This analysis benefits from earlier analyses of conventional spacecraft–quasar ΔDOR by Brooks Thomas, Sien Wu, and Bob Treuhaft. The authors thank Roger Linfield, Bill Folkner, Sam Thurman, and Lincoln Wood for their helpful comments on a draft of this article.

References

[1] R. N. Treuhaft and S. T. Lowe, "Nanoradian VLBI Tracking for Deep Space Navigation," paper AIAA 90-2939, *Proceedings of the AIAA/AAS Astrodynamics Conference*, pp. 587–589, Part 2, Portland, Oregon, August 20–22, 1990.

[2] W. Folkner and J. Border, "Orbiter–Orbiter and Orbiter–Lander Tracking Using Common-Beam Interferometry," paper 90-2906, *Proceedings of the AIAA/AAS Astrodynamics Conference*, Part 1, pp. 355–363, Portland, Oregon, August 20–22, 1990.

[3] D. M. Tralli and S. M. Lichten, "Stochastic Estimation of Tropospheric Path Delays in Global Positioning System Geodetic Measurements," *Bulletin Geodesique*, vol. 64, pp. 127–159, 1990.

[4] T. H. Dixon and W. S. Kornreich, "Some Tests of Wet Tropospheric Calibration for the CASA Uno Global Positioning System Experiment," *Geophys. Res. Letters*, vol. 17, pp. 203–206, March 1990.

[5] R. N. Treuhaft and G. E. Lanyi, "The Effect of the Dynamic Wet Troposphere on Radio Interferometric Measurements," *Radio Sci.*, vol. 22, pp. 251–265, 1987.

[6] P. S. Callahan, "Ionospheric Variations Affecting Altimeter Measurements: A Brief Synopsis," *Marine Geodesy*, vol. 8, pp. 249–263, 1984.

[7] R. D. Kahn and J. S. Border, "Precise Interferometric Tracking of Spacecraft at Low Sun–Earth–Probe Angles," paper AIAA-88-0572, presented at Aerospace Sciences Meeting, Reno, Nevada, January 11–14, 1988.

[8] R. Woo and J. W. Armstrong, "Spacecraft Radio Scattering Observations of the Power Spectrum of Electron Density Fluctuations in the Solar Wind," *J. Geophys. Res.*, vol. 84, p. 7288, 1979.

[9] R. P. Malla and S. C. Wu, "GPS Inferred Geocentric Reference Frame for Satellite Positioning and Navigation," *Bulletin Geodesique*, vol. 63, pp. 263–279, 1989.

[10] A. P. Freedman, "Determination of Earth Orientation Using the Global Positioning System," *TDA Progress Report 42-99*, vol. July–September 1989, pp. 1–11, November 15, 1989.

[11] D. Jones, R. Dewey, C. Gwinn, and M. Davis, "Mark III VLBI Astrometry of Pulsars," *IAU Colloquium 131, Radio Interferometry: Theory, Techniques, and Applications*, ed. T. Cornwell, Socorro, New Mexico, October 1990.

[12] R. Linfield, "Using Planetary Occultations of Radio Sources for Frame Tie Measurements; Part 1: Motivation and Search for Events," *TDA Progress Report 42-103*, vol. July–September 1990, pp. 1–13, November 15, 1990.

[13] M. Finger and W. Folkner, "A Determination of the Radio-Planetary Frame-Tie and the DSN Tracking Station Locations," paper 90-2905, *Proceedings of the AIAA/AAS Astrodynamics Conference*, Part 1, Portland, Oregon, pp. 335–353, August 20–22, 1990.

[14] J. Border and W. M. Folkner, "Differential Spacecraft Tracking by Interferometry," paper CNES-89-145, *Proceedings of the CNES International Symposium on Space Dynamics*, Toulouse, France, pp. 6–10, November 1989.

[15] A. Konopliv and L. Wood, "High Accuracy Mars Approach Navigation with Radiometric and Optical Data," paper AIAA 90-2907, *Proceedings of the AIAA/AAS Astrodynamics Conference*, Part 1, Portland, Oregon, pp. 364–376, August 20–22, 1990.

[16] R. D. Kahn, W. M. Folkner, C. D. Edwards, and A. Vijayaraghavan, "Position Determination of Spacecraft at Mars Using Earth-Based Differential Tracking," paper AAS 91-502, presented at AAS/AIAA Astrodynamics Specialist Conference, Durango, Colorado, August 19–22, 1991.

Table 1. Observation description.

Observation sequence	Time, sec
Spacecraft A	60
Slew time	60
Spacecraft B	120
Slew time	60
Spacecraft A	60

Observation geometry	
Mean elevation angle	20 deg
Angular separation	0–20 deg, in elevation direction at both stations
Projected baseline length	6,000 km

	Spacecraft signal spectrum	
	Case 1, X-band	Case 2, Ka-band
Carrier frequency	8.4 GHz	32.0 GHz
DOR tone spacing	±20 MHz	±125 MHz
Received DOR tone SNR	25.6 dB-Hz	25.6 dB-Hz

Table 2. Error-modeling assumptions.

Spacecraft SNR	
DOR bandwidth	
Case 1, X-band	40 MHz
Case 2, Ka-band	250 MHz
P_{tone}/N_0	25.57 dB-Hz
Instrumentation	
Single-channel dispersive phase error	0.001 cyc
Clock stability	
Time between spacecraft scans	150 sec
Allan variance	1×10^{-14}
Static troposphere	
Zenith troposphere uncertainty	1 cm
Mean elevation angle	20 deg
Fluctuating troposphere	
Treuhaft–Lanyi model	(as per [8])
Static ionosphere	
Zenith ionosphere uncertainty	5 TEC units
Frequency	
Case 1, X-band	8.4 GHz
Case 2, Ka-band	32 GHz
Mean elevation angle	20 deg
Fluctuating ionosphere	
RMS TEC fluctuation	0.5 TEC units
Baseline	
Station location uncertainty	3 cm
Earth orientation uncertainty	10 nrad
Radio-planetary frame tie	
Frame-tie error	25 nrad
Solar plasma	
Sun–Earth–probe angle	20 deg

Table 3. Error budget for X-band spacecraft–spacecraft ΔDOR.

Angular separation, deg	Spacecraft SNR, nrad	Instrumentation, nrad	Clock stability, nrad	Troposphere, nrad	Ionosphere, nrad	Baseline, nrad	Solar plasma, nrad	Frame tie, nrad	RSS, nrad
0.10	1.91	3.54	0.11	0.67	0.67	0.02	<0.50	0.22	4.16
1.00	1.91	3.54	0.11	0.76	0.76	0.21	0.50	0.44	4.22
2.00	1.91	3.54	0.11	0.97	0.99	0.43	0.50	0.87	4.39
4.00	1.91	3.54	0.11	1.55	1.59	0.86	0.50	1.75	5.01
8.00	1.91	3.54	0.11	2.95	2.95	1.71	0.50	3.49	7.00
10.00	1.91	3.54	0.11	3.74	3.64	2.14	0.50	4.36	8.20
20.00	1.91	3.54	0.11	9.29	7.00	4.28	0.50	8.73	15.69

Table 4. Error budget for Ka-band spacecraft–spacecraft ΔDOR.

Anglular separation, deg	Spacecraft SNR, nrad	Instrumentation, nrad	Clock stability, nrad	Troposphere, nrad	Ionosphere, nrad	Baseline, nrad	Solar plasma, nrad	Frame tie, nrad	RSS, nrad
0.10	0.31	0.57	0.11	0.67	0.05	0.02	<0.03	0.22	0.94
1.00	0.31	0.57	0.11	0.76	0.05	0.21	0.03	0.44	1.11
2.00	0.31	0.57	0.11	0.97	0.07	0.43	0.03	0.87	1.52
4.00	0.31	0.57	0.11	1.55	0.11	0.86	0.03	1.75	2.57
8.00	0.31	0.57	0.11	2.95	0.20	1.71	0.03	3.49	4.93
10.00	0.31	0.57	0.11	3.74	0.25	2.14	0.03	4.36	6.17
20.00	0.31	0.57	0.11	9.29	0.48	4.28	0.03	8.73	13.47

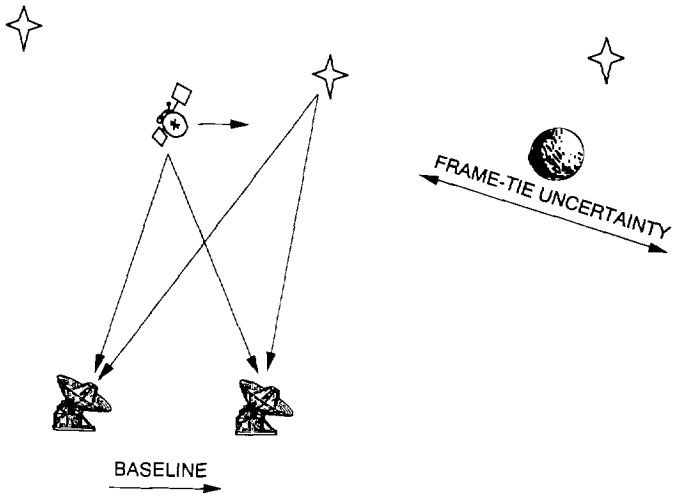

Fig. 1. Conventional ΔDOR provides a determination of the angular position of a spacecraft relative to the reference frame of distant quasars. Uncertainty in the position of the target planet in this reference frame represents an important navigation error source.

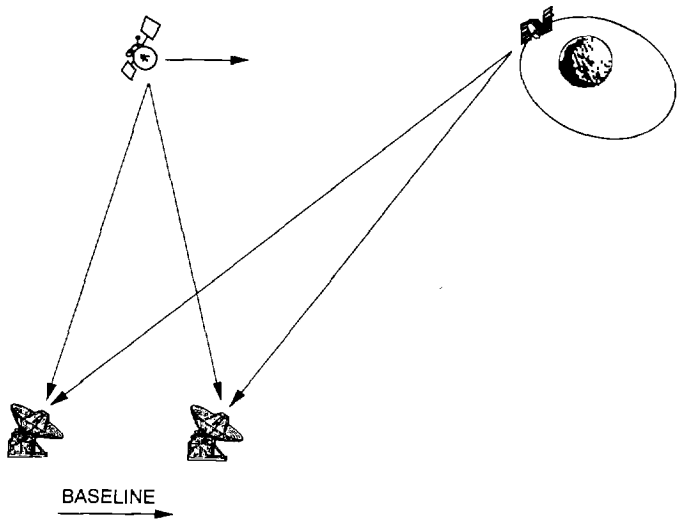

Fig. 2. Spacecraft–spacecraft ΔDOR observations between an approach spacecraft and a planetary orbiter provide direct planet-relative approach navigation.

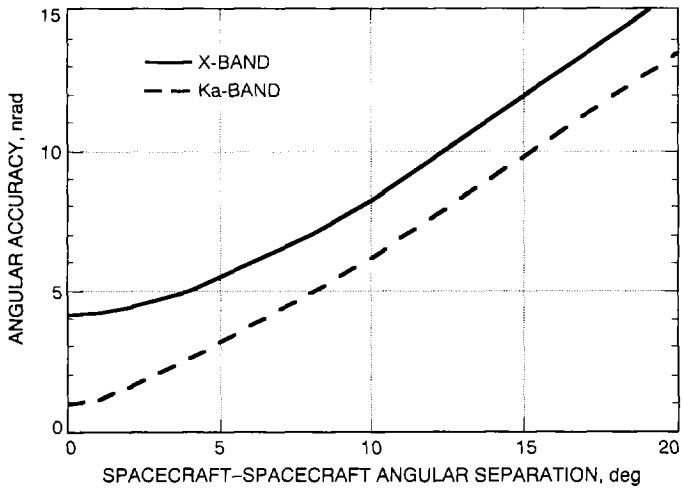

Fig. 3. Angular accuracy versus spacecraft angular separation for X-band and Ka-band spacecraft–spacecraft ΔDOR.